Applied Surface Science 529 (2020) 146995

Contents lists available at ScienceDirect

Applied Surface Science

journal homepage: www.elsevier.com/locate/apsusc

Full Length Article

The effect of oxygen flow rate on metal–insulator transition (MIT) characteristics of vanadium dioxide (VO_2) thin films by pulsed laser deposition (PLD)

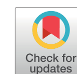

Syed A. Bukhari[a], Sooraj Kumar[b], Pawan Kumar[c], Sarang P. Gumfekar[a,d], Hyun-Joong Chung[a], Thomas Thundat[a,e], Ankur Goswami[b,*]

[a] Department of Chemical and Materials Engineering, University of Alberta, Edmonton, AB T6G1H9, Canada
[b] Department of Materials Science and Engineering, Indian Institute of Technology, Delhi, Hauz Khas, New Delhi 110016, India
[c] Department of Electrical and Computer Engineering, University of Alberta, Edmonton, AB T6G1H9, Canada
[d] Department of Chemical Engineering, Indian Institute of Technology, Ropar, Punjab 140001, India
[e] Department of Chemical and Biological Engineering, State University of New York, Buffalo, 310 Furnas Hall Buffalo, NY 14260, USA

ARTICLE INFO

Keywords:
Vanadium dioxide
Pulsed laser deposition
Metal–insulator transition

ABSTRACT

Vanadium dioxide (VO_2), because of its unique metal–insulator phase transion around room temperature, has enormous potential for applications in thermochromic, electrochromic, microbolometery, and non-volatile switches. However, obtaining phase-pure VO_2 has been challenging due to its narrow window of thermodynamic stability. Pulsed laser deposition (PLD) is considered to be one of the most promising technique to deposit phase-pure VO_2 thin films. While optimizing PLD processing parameters, (such as oxygen pressure (P_{O2}), substrate temperature (T_s), laser energy (E_L), target-substrate distance ($d_{T\text{-}S}$), and laser repetition rate (RR)) is crucial, and their effects have been reported, the effect of gas flow rate (Q_{O2}) has been largely neglected. Since the Q_{O2} and P_{O2} of the PLD system are intertwined at the outset, most reports are focused only on either Q_{O2} or P_{O2}. We report on the effect of gas flow rate under constant $P_{O2,}$ on the quality of the VO_2 thin films. Controlling flow rate affected the resistivity contrast between the metallic and insulator phases, the temperature ranges of the transition, and the width of hysteresis. We anticipate that this study will help set the standard for obtaining high quality VO_2 thin films.

1. Introduction

A large number of transition metal oxides exhibit metal to insulator transition (MIT) when it is activated by external stimuli such as thermal, pressure, optical irradiation, electric and magnetic field [1–5]. This transition causes drastic changes in electrical, mechanical, magnetic, optical and thermal properties of phase change metal oxides [6–10]. Vanadium dioxide (VO_2) is one such material which shows this type of first-order transition where material undergoes insulator to metal transition, known as Mott transition or Peierls transition in literature, although long-lasting debate persists about the type of transition [11,12]. VO_2 is a strongly correlated system having several polymorphs which are comprised of VO_2 (M1), VO_2(R), VO_2(A) and VO_2(B) phases predominantly [13]. Owing to the strong electron–electron correlation they exhibit many interesting electrical, mechanical, optical and chemical properties due to their completely different crystalline and electronic structures despite having the same chemical formula. Among all the above phases, the VO_2 (M1) and VO_2 (R) phases have caught tremendous attention in the last several decades for their insulator (monoclinic-$P2_1/c$) to metal (tetragonal-$P4_2/mnm$) transitions occurings ideally at 68 °C where they undergo a change in resistance of more than three orders of magnitude [14]. This property of VO_2 is found in a plethora of exotic applications such as smart windows [15], frequency tuning devices [16,17], electronic and resistive switches [18], non-volatile memory [19], microbolometers [20], gas and strain sensing [21].

Despite having significant technological applications, obtaining phase pure VO_2 is still a challenge because of its narrow range of stability in the VO_2 phase of V-O phase diagram [22]. Although there have been significant efforts which devoted to synthesize and stabilize different polymorphs of VO_2, both in bulk and thin-film form, the effect of a large numbers of parameters still need to be addressed [23,24].

* Corresponding author.
E-mail address: agoswami@mse.iitd.ac.in (A. Goswami).

https://doi.org/10.1016/j.apsusc.2020.146995
Received 14 April 2020; Received in revised form 6 June 2020; Accepted 15 June 2020
Available online 19 June 2020
0169-4332/ © 2020 Elsevier B.V. All rights reserved.

Compared to bulk, the inhomogeneity in thin films of VO_2 can cause strain which modifies electronic and lattice states and provides an extra degrees of freedom to tune the MIT characteristics. Since our effort is to address the thin film form of VO_2, we will restrict the discussions on parameter optimization to the VO_2 thin film only. For instance, the partial pressure of oxygen is one of the major parameters which dramatically alter the phase stability of vanadium dioxide due to the multivalent states of vanadium. Similarly, the temperature of the substrate also plays a crucial role in the formation of different phases and polymorphs (such as VO_2 (A), VO_2 (B), VO_2 (M1), VO_2 (R)) [13,25]. Stabilized phases of these films provide unique crystal structure and properties. Several deposition techniques have been adopted in literature to obtain high quality VO_2 such as chemical vapor deposition (CVD) [26], sputtering (both DC and RF) [27–29] and pulsed laser deposition (PLD) [30,31].

Among all the above mentioned thin film deposition methods, PLD allows distinct advantages to fabricate varieties of materials by stoichiometrically transferring target material to the substrate and employing a high energy focused laser beam onto the target by creating a highly directional plasma plume towards the substrate [32]. However, gas pressure (P_{O2}), substrate temperature (T_s), laser energy (E_L), target-substrate distance ($d_{T\text{-}S}$), and laser repetition rate (RR), are equally important parameters to optimize the obtained phase grown on the substrate. Several efforts have been put forth to deposit VO_2 film by employing the PLD technique using vanadium metal [33], vanadium oxide (V_2O_3 [34], V_2O_5 [35], and VO_2 [36]) as a target material. In most of the reports obtaining phase-pure VO_2 involves a two step processes wherein film is first deposited, followed by an insitu or exsitu controlled annealing or by rapid thermal annealing (RTA) [37] in oxygen at a set pressure.

Recently few studies have been reported employing the PLD technique where 25–30 nm VO_2 films (both polycrystalline and epitaxial form) were grown using a vanadium metal target on amorphous (Si/SiO_2) and single-crystal substrates (silicon and sapphire) in a one step process [38]. McGee et al. extensively studied the optimization of vanadium oxide growth on amorphous thermal oxide (Si/SiO_2) substrate using vanadium metal as a target by adopting the Taguchi method of design of experiment (DOE) taking four different experimental factors into account i.e. P_{O2}, T_s, $d_{T\text{-}S}$ and E_L [39]. They found oxygen pressure to be the most influential among all the other parameters in the case of obtaining phase pure VO_2. They prescribed P_{O2} = 50 mTorr, T_s = 600 °C, $d_{T\text{-}S}$ = 31 mm and E_L = 2.6 J/cm^2 to be the optimum parameters to obtain the VO_2 (M1) phase which undergoes the first-order transition. Bhardwaj *et al.* further studied the effect of P_{O2} while keeping other parameters constant and found the range of P_{O2} to obtain different valence states of vanadium oxides (such as V_2O_3, VO_2, and V_2O_5) and reaffirm the same parameters to obtain phase pure VO_2 (M1) as suggested by McGee et al. [25].

In both of the above cases it can be argued that P_{O2} is the only influential parameter to obtain the desired phase of VO_2, as also has been addressed in many past works of literature, although, using different deposition techniques [25,40]. Similarly, there are reports emphasizing the dependence of gas flow rate (Q_{O2}) in obtaining phase-pure VO_2 (M1) [41,42]. Most of these reports where the flow rate is the variable parameter, the pressure was not monitored It is obvious that gas pressure in a controlled volume is dependent on flow rate and pumping speed. It is also obvious that by keeping the pumping speed constant, one can manipulate the gas pressure by changing the flow rate. Therefore, all the reports on the optimization of depositing VO_2 by manipulating the gas flow rate (Q_{O2}) are analogous to the tuning the gas pressure only as the exact gas pressure was not reported many of the above cases [43]. Here we argue that by keeping the gas pressure constant (P_{O2} ~ 50 mTorr), one can still manipulate the vanadium oxide phase by changing the gas flow rate (Q_{O2}). It is quite obvious to get puzzled because gas pressure is the major important factor for any oxide deposition in any physical vapor deposition processes regardless of flow rate since gas pressure dictates the number of gas molecules required for the reaction. However, we found a counter-intuitive observation. We observed that there is a critical flow rate range at which the desired phase of VO_2 can be achieved even though the required gas pressure is maintained in the chamber. However, below and above that critical flow rate range the obtained phase and microstructure deviates either from the desired VO_2 phase or from the desired microstructure.

Therefore, we systematically studied the optimization of the VO_2 phase on an amorphous thermal oxide (Si/SiO_2) substrate by varying Q_{O2} and keeping P_{O2} (~50 mTorr), and the other parameters (T_s, $d_{T\text{-}S}$, E_L) constant. In order to keep P_{O2} constant while varying the Q_{O2} the pumping speed was altered accordingly.

2. Experimental

2.1. Thin films deposition

Vanadium oxide films were deposited with PLD in an oxygen atmosphere (99.993% purity, Praxair) using a vanadium metal (99.9% purity, American Elements) circular disc (1″ dia 0.250″ thickness) as a target. The deposition chamber (Excel Instruments, Mumbai, India) is schematically shown in Fig. 1. The vanadium target was mounted on a metallic circular disc which was further attached with a stepper motor in order to provide a rotating and oscillating motion so that the laser ablates the material from all areas of the target material. The target-substrate distance was kept 31 mm. Laser pulses with a 20 ns pulse width from a krypton fluoride (KrF, λ = 248 nm) excimer laser (Coherent, GmbH) were directed at the target with a repetition rate of 10 Hz. The laser spot size of 1–3 mm was maintained on the target with a constant energy density of 2.6 J/cm^2. The deposition time was kept at15 min for all depositions on the thermal oxide (Si/SiO_2 (1 μm)) wafer. Before deposition, the substrates were cleansed with piranha, followed by sonication in milli-Q water, rinsed in ethanol, and dried with nitrogen. The substrate's size was 12.5 × 12.5 mm^2. The chamber was evacuated to 1.5 × 10^{-6} mbar and it remained under pumping for at least 3 h. The substrate heating turned on when the vacuum level dropped below 10^{-5} torr. After that, oxygen was introduced into the system with a fine-tuned flow rate to keep the pressure in the chamber constant for an hour. A total of seven numbers of film were deposited with seven different flow rates (i.e. 0.5, 1, 5, 10, 30, 50 and 90 sccm) of oxygen. The pressure in the chamber was maintained at 50 mTorr for seven samples. Once the deposition was done, each sample was cooled to room temperature naturally before it was taken out.

2.2. Characterization techniques

2.2.1. X-ray diffraction (XRD)

Thin-film samples were characterized by XRD (Rigaku XRD Ultima IV) diffractometer at glancing angle mode, setting an incident angle at 0.5° using CuK_α (λ = 1.5418 A^o) as a source. The experiment was done at 25 °C. The low incident angle was required because the thickness of VO_2 films is very small and a small incident angle would reduce the possibility of obtaining a background signal in the spectrum because of the substrate.

2.2.2. Scanning electron microscopy for microstructure analysis

SEM analysis was carried out using Zeiss Sigma (Gemie) FE-SEM. Thin films were coated with 10 nm sputtered gold before imaging in order to avoid a charging effect. It is important to mention SEM was performed after all the electrical measurements were completed.

2.2.3. Surface analysis by AFM

A Dimension Fast Scan Atomic Force Microscope (Bruker Nanoscience division, Santa Barbara, CA, USA) was used to map the surface topography of the films using intermittent contact mode. Cantilevers with the tips coated with Pt-Ir (SCM-PIT) with a spring

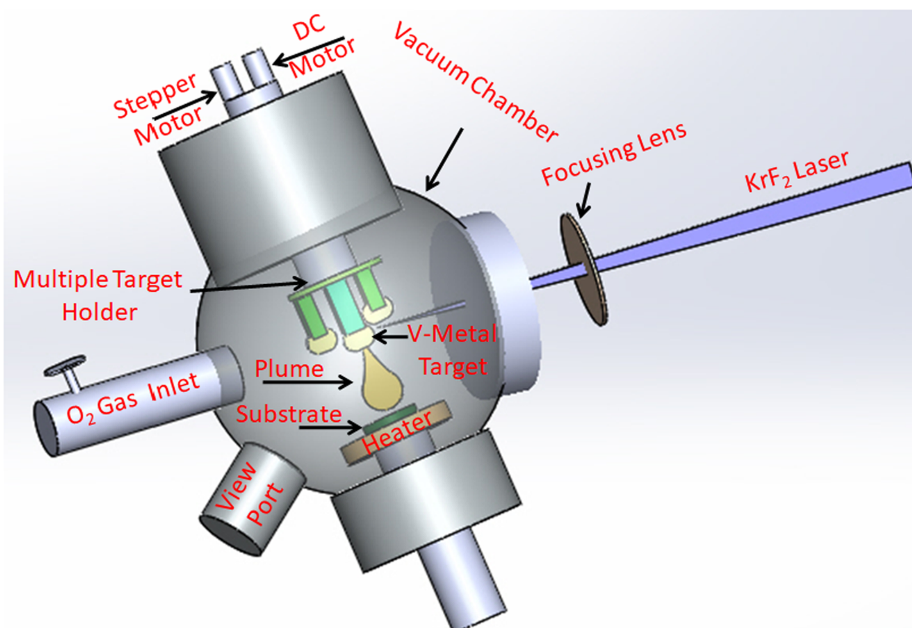

Fig. 1. Schematic of the PLD experimental setup, including the laser path and the PLD chamber.

constant of 3.6 N/m and a resonant frequency of 69 kHz were used for obtaining surface morphology. Obtained images were processed using Nanoscope analysis software to determine the average surface roughness of the scanned area.

2.2.4. X-ray photoelectron spectroscopy

An XPS Spectrometer (Kratos AXIS Ultra) was used to analyze the optimization of the oxidation states of thin films. A total of seven VO_2 films were deposited under the same pressure and temperature conditions, only changing the oxygen flow rate. The shift in the peak positions of the XPS spectra of oxygen-rich and oxygen-poor samples was studied as a function of the oxygen flow rate. The surface/sub-surface (10 nm) chemical composition and oxidation state were determined using X-ray photoelectron spectroscopy (XPS) acquired on Axis-Ultra, Kratos Analytical instrument equipped with monochromatic Al-Kα source (15 kV, 50 W) and photon energy of 1486.7 eV under an ultrahigh vacuum, UHV (10^{-8} Torr). The binding energy of C1s carbons (284.8 eV) of adventitious hydrocarbons was used as the standard, and the binding energy of other elements is assigned relative to the C1s peak (carbon correction). The XPS data was deconvoluted into various peak components using CasaXPS.

2.2.5. Micro-Raman spectroscopy

Micro-Raman spectroscopy was performed on vanadium dioxide thin films using the DXR2 Smart Raman spectrometer. The measurements were performed using 532 nm laser light operating at10 mW power with an exposure collection time of 10 s. In all the experiments a 100 X objective was used. The experiments were performed at room temperature.

2.2.6. Electrical measurement

Electrical contacts were made using the aluminum hard mask on samples by employing the e-beam evaporation technique by depositing Ti/Au (20/80 nm). An array of circular contact pads was made using the hard mask which is 0.5 mm in diameter and 1 mm apart. In order to investigate the magnitude, shape and width of the insulator to metal transition, Keithley 2602B source meter unit was used. Resistance was monitored as a function of temperature in two probe configurations. A fully integrated Signatone 1160 series probe station was used to provide controlled heating. Resistance was measured in voltage-controlled mode by applying 0.5 V to the sample Thermo-Scientific chiller was used to extract out the extra heat from the sample stage. Resistance vs temperature data was acquired and plotted from 10 to 100 °C for both heating and cooling cycles. The samples were heated at a controlled rate of 2 °C/ min with an equilibrium time of 3 min at each temperature before taking a measurement. Each measurement is an average of five measurements taken at a constant temperature.

3. Results and discussion

3.1. X-ray diffraction analysis

The XRD of the deposited seven films, grown in different flow rate conditions, was carried out and shown in Fig. 2. The majority of the obtained peaks were matched with the VO_2 (M1) phase having a space group of $P2_1/c$ (JCPDS # 82-0661). However, there are some possible

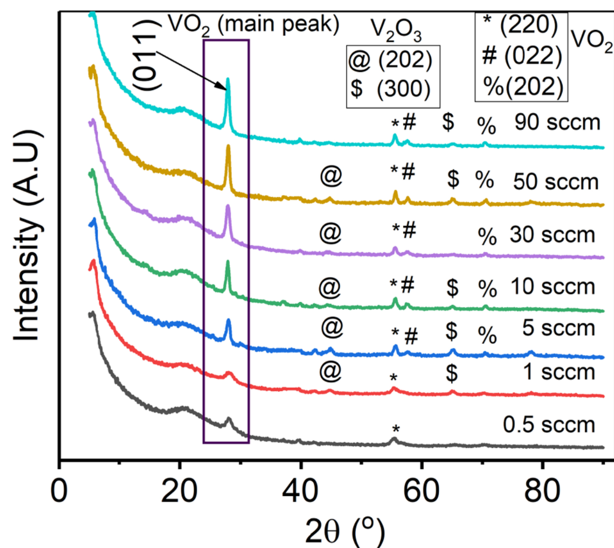

Fig. 2. XRD spectra of vanadium dioxide films deposited by PLD on thermal oxide (Si/SiO_2) substrates at different oxygen flow rates but at the same pressure (p_{O2} = 50 mTorr).

V_2O_3 impurity peaks which can be seen in most of the samples similar to the space group of $R\bar{3}c$ V_2O_3 (JCPDS# 84-0319). It is observed that film grown on a low flow rate condition does not show sufficient crystallinity. However, as the flow rate increases, (0 1 1) plane becomes sharper, and (2 2 0) and (0 2 2) planes become more prominent, which shows an increment in the crystalline nature of the film. For instance, a tiny peak appears at 27.88° with a flow rate of 0.5 sccm, which becomes more prominent with an increasing O_2 flow rate at 5 sccm and becomes sharper with further increment. As expected, all the films are polycrystalline in nature as they were deposited on the amorphous thermal oxide substrate. The intensity of the peak is found to be increased as the flow rate of oxygen was enhanced. The broader peak also corresponds to the smaller crystalline size (as per Scherrer equation) whereas the crystalline size becomes larger with a higher flow rate.

3.2. Raman studies

In order to confirm further, Raman measurements were carried out on the film synthesized in different flow rate conditions. The monoclinic VO_2(M1) phase normally has 18 phonon modes in the Raman spectra among which 9 modes correspond to A_g symmetry and rest are of B_g symmetry [50]. On the other hand, the rutile phase normally shows 4 Raman modes i.e. A_{1g}, B_{1g}, B_{2g} and E_g which are broad in nature and found to be at 240, 390, 510 and 625 cm^{-1}. Nevertheless, the intensity of Raman modes in the rutile phase is low compared to the monoclinic phase and is not present in the spectra shown here. The signature peak of VO_2 in Raman spectra is mostly A_g modes which correspond to V-O-V bending modes (< 400 cm^{-1}) and stretching modes (400–800 cm^{-1}) as depicted in Fig. 3 and also reported in various literature [13,25]. It is observed that the peak corresponds to A_g (at 193, 223 cm^{-1} and 616 cm^{-1}) are not prominent in the low flow rate regime i.e. 0.5 and 1 sccm. However, as the flow rate increases, these peaks became more evident. The peak at 304 and 388 cm^{-1} (both corresponds to A_g) also become evident from the 30 sccm flow rate.

3.3. Microstructure analysis

Fig. 4 illustrates the SEM micrographs of the samples deposited under different oxygen flow rate conditions. It is observed from the micrograph that at the initial flow rate condition the film appears to be amorphous as it lacks features as shown in Fig. 4(a). However, with increasing flow rate the fine-grain morphology started appearing and became quite evident in Fig. 4(d) when the flow rate increased to 5 sccm. From 5 to 30 sccm the fine-grain morphology persisted; however, with increasing flow rate the grains started growing as appeared in Fig. 4(f) and (g). These microstructures also support the XRD data where at low flow rate regime (0.5 to 5 sccm) the broad peak (0 1 1) was observed; however, as the grain started growing, narrow to narrower (low to lower full width-half-maximum (FWHM)) a peak started appearing from an intermediate (10 to 30 sccm) to higher flow rate (50 to 90 sccm) regime respectively. The evolution of the microstructure with an increasing flow rate might be due to the increasing nucleus density owing to increased supersaturation [45].

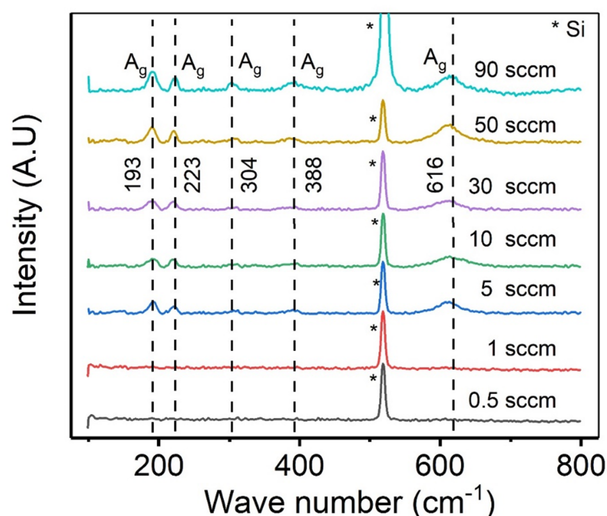

Fig. 3. Raman spectra of vanadium dioxide (VO_2) at different O_2 flow rates but at the same pressure (p_{O2} = 50 mTorr).

3.4. Surface morphology and roughness analysis by AFM

Surface morphology and roughness were further characterized by the AFM technique. In pulsed laser deposition predominantly Volmer-Weber growth (island growth), a mechanism dominates when the substrate is amorphous in nature. At low oxygen flow rate (0.5 sccm and 1 sccm) very small crystalline particles nucleate as shown in Fig. 5(a) and (b) suggesting small islands are forming due to supersaturation when the plasma plume hits the substrate. Hence, the deposited films exhibit moderate roughness. With increasing flow rate, it is observed that grain growth started occurring as depicted in Fig. 5(c) because of the increase in the rate of surface diffusion. A higher gas flow rate possibly replenished the substrate surface to accommodate and grow more adatoms on the substrate. These results slightly increase the roughness parameter. However, with further increasing the flow rate (Q_{o2} = 10 and 30 sccm), which is the intermediate regime, an interesting morphology appeared, where in addition to the island growth, a layer growth mechanism (known as Frank-van der Merwe) also start evolving (Fig. 5(d) and (e)) and thereby allowed the supersaturate vapor to condense in the larger area (contrary to the lower flow rate). Therefore, the roughness of the film reduced in this intermediate flow rate regime However, with further increases to the flow rate range (50 and 90 sccm), large grain growth or coarsening was observed, thereby increasing the roughness of the film. Fig. 5(h) shows the variation of the roughness parameters of the film with the function of the oxygen flow rate. This trend indicates there is a critical regime of flow rate where the morphology of the sample found to be smoother in comparison to the samples grown in lower or higher flow rates.

3.5. XPS analysis

X-ray photoelectron spectroscopy (XPS) was used to determine the surface chemical composition and binding energies of constituting elements. Fig. 5(a) and Fig. S1(a) (see supplementary section) shows the XPS survey scan of material for elemental analysis which exhibits characteristics $V2_p$, $O1_s$ peaks along with low and high energy core level peaks (OKLL, $V3_s$). The presence of these peaks validates the presence of all the composing elements. Sub-quantitative analysis using peak to peak intensity ratio demonstrates a $V2_p$ to $O1_s$ percentage atomic ratio at 0.5 sccm flow rate to be 36.4/63.6, which is in between the theoretical ratio for VO_2 (33.3/66.7) and V_2O_3 (40.0/60.0) suggesting the presence of both components in the material. After increasing the flow rate to 1.0 sccm, a slight decrease in oxygen content was corroborated to the transition of VO_2 ($^{4+}$) to V_2O_3 ($^{3+}$). However, a further increase in flow rate (5.0, 10.0 and 30.0 sccm) lead to an increase in oxygen content (36.6/63.4, 29.7/70.3, 30.7/69.3) approaching toward the atomic ratio of V_2O_5 (28.6/71.4) (Fig. 6(a), Table 1). Interestingly, at 50 sccm the oxygen content decreased slightly, demonstrating the partial transformation of VO_2 to V_2O_3. Again at 90 sccm, the oxygen content increased (30.4/69.6). The core-level high-resolution XPS spectra of materials in the $V2_p$ region show two major peaks assigned to $V2p_{3/2}$ and $V2p_{1/2}$ orbital splitting. Each $V2_p$ peak component can be deconvoluted into various peak components showing the existence of vanadium in a variable oxidation state (Fig. 6(b)).

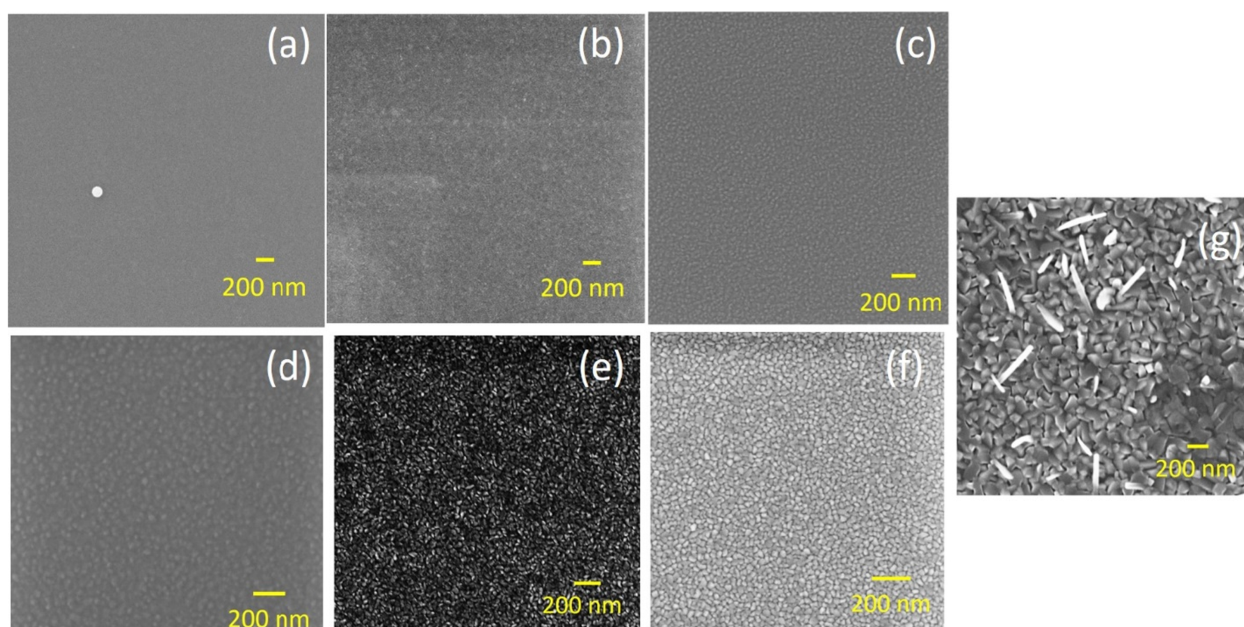

Fig. 4. SEM micrograph of vanadium oxide deposited at (a) 0.5 sccm, (b) 1 sccm, (c) 5 sccm, (d) 10 sccm, (e) 30 sccm, (f) 50 sccm, (g) 90 sccm O_2 flow rate.

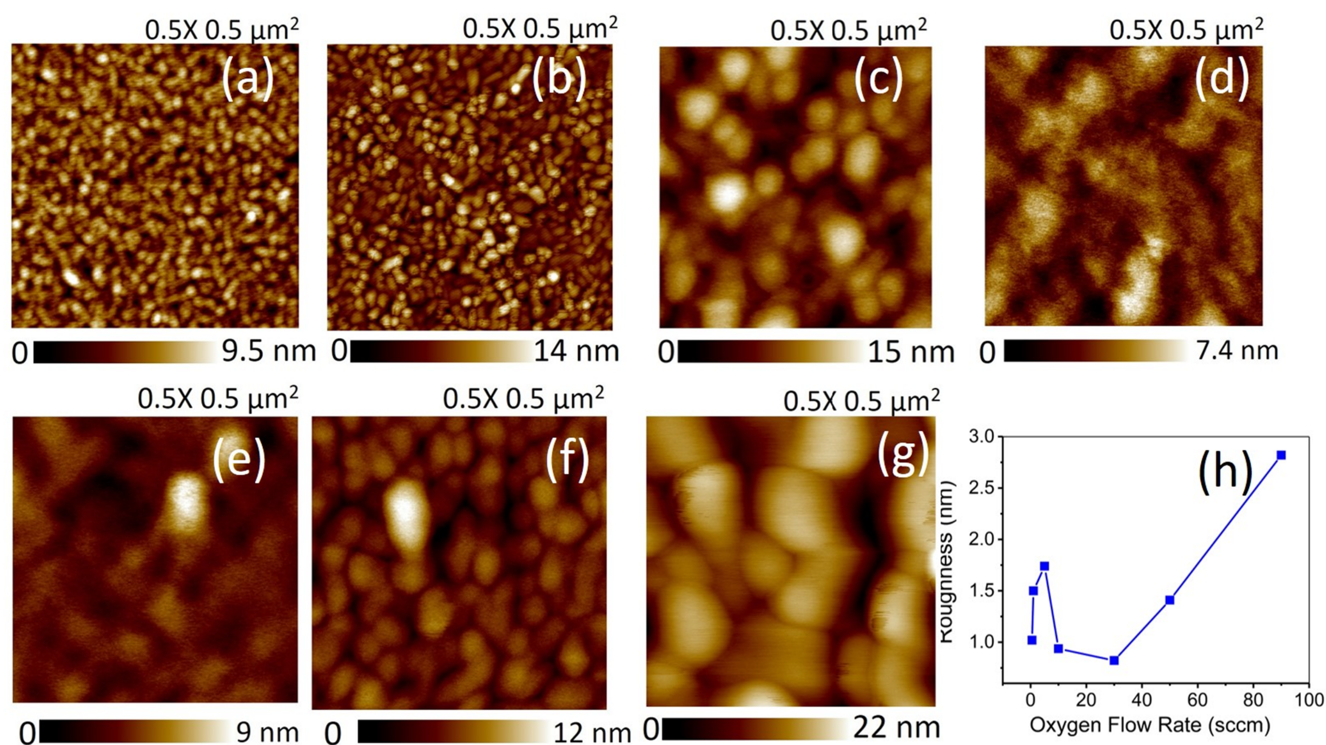

Fig. 5. Roughness of vanadium oxide thin film deposited under different oxygen flow rates i.e. (a) 0.5 sccm, (b) 1 sccm, (c) 5 sccm, (d) 10 sccm, (e) 30 sccm, (g) 50 sccm, (f) 90 sccm O_2 flow rate. (h) Variation of average surface roughness is plotted as a function of flow rate. Bare thermal oxide (Si/SiO_2) roughness 0.174 nm (data not shown).

The deconvoluted $V2p_{3/2}$ peak of VO_2 thin film at 0.5 sccm flow rate show two peak components located at 515.9 and 517.1 eV binding energy corroborated to V_2O_3 and VO_2 present as V^{3+} and V^{4+} oxidation state. Upon increasing the flow rate, the contribution of the V^{3+} peak was decreased suggesting a transition of V_2O_3 into a higher oxidation state (VO_2 and V_2O_5). At 5.0, 10 and 30 sccm a shoulder peak at BE= 517.8 eV originated from a V^{5+} oxidation state of V_2O_5 was observed, which increased in the order of flow rate indicating that a small fraction get converted into V_2O_5. However further increase in flow rate does not reveal any existence of a V^{5+} state, rather contribution of V^{3+} peak component was increased. This observation suggests that with increased flow rate oxygen molecules do not get the opportunity to adsorb/react with the material. The observed pattern of the relative contribution of each component is well-matched with the observed atomic percentage calculated from the XPS survey scan. Further, evidence of flow rate dependent transformation of the oxidation state comes from the HR-XPS spectra of materials in the $O1_s$region (Fig. 6(c)).

The HR-XPS spectra of all the samples exhibit double-peak structure

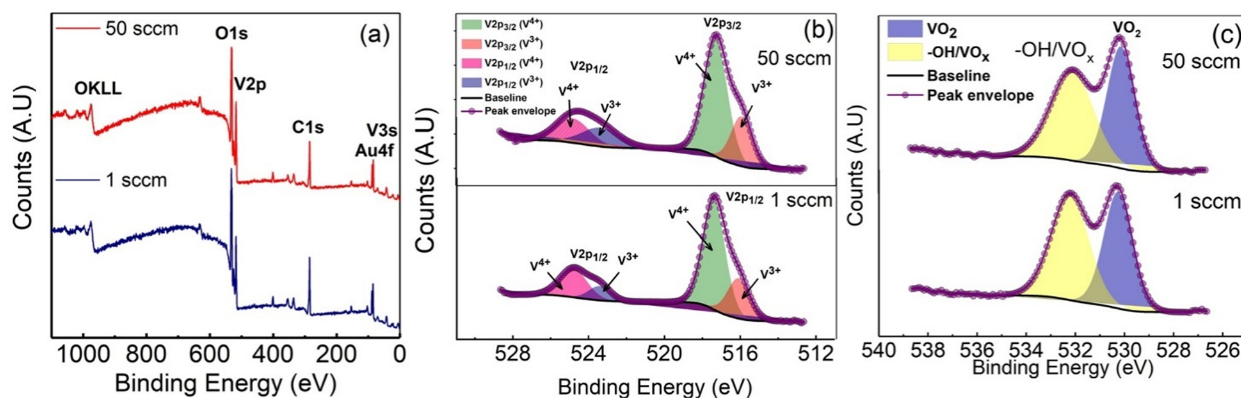

Fig. 6. (a) XPS survey scan of VO_2 thin film grown at two different flow rates i.e. 1 and 50 sccm, (b) Core-level HR-XPS spectra of VO_2 samples in V2p region demonstrating various oxidation states and relative contribution (c) HR-XPS spectra of VO_2 samples in O1s region at 1 and 50 sccm.

Table 1
XPS elemental analysis of VO_2 thin film showing the change in the chemical composition of materials as a function of flow rate.

S. No.	Film deposited at different flow rates (sccm)	V2p/O1s	$V^{5+}/V^{4+}/V^{3+}$	–OH + VO_X/VO_2
1.	0.5	34.6/63.6	(−)/40.2/59.8	44.5/55.5
2.	1.0	43.4/56.6	(−)/70.5/29.5	49.4/50.6
3.	5.0	36.6/63.4	8.8/63.2/28.0	64.3/35.7
4.	10	29.7/70.3	28.0/44.0/31.0	72.7/27.3
5.	30	30.7/63.9	36.0/45.6/18.4	70.3/29.7
6.	50	42.5/57.5	(−)/60.8/39.2	47.5/52.5
7.	90	30.4/69.6	(−)/48.1/51.9	48.1/51.9

and can be deconvoluted into two well-separated peak components centered at 530.2 and 532.1 eV. The peak at 530.2 eV was originated due to lattice bounded oxygen of VO_2 while another peak at 532.1 eV was observed due to cumulative contribution of non-lattice surface oxygen (–OH) and oxygen bonded with vanadium in higher oxidation state V^{5+} (V_2O_5/VO_x). It can be seen from spectra that the relative contribution of oxygen peaks from VO_2 was decreased (from 55.5 to 29.7 for 0.5–30 sccm) while –OH/VO_x peak was increased up to 30 sccm, and agreed well with $V2_p$ XPS. For the 50 and 90 sccm flow rate, the VO_2 contribution remains stable to 51–52% as expected from the $V2_p$XPS spectrum.

3.6. Insulator to metal transition

Insulator to metal transition was confirmed with a two probe resistance measurement as a function of temperature. The magnitude, shape, and width of the transition were studied as a function of the oxygen flow rate and tabulated in Table 2. Normalized resistance vs temperature data for all the samples deposited on various flow rates are shown in Fig. 7. No insulating to metallic state transition was seen for flow rates of 0.5 and 1 sccm [Fig. 7(a)]. This is because neither sample shows appreciable VO_2 (M1) phase formations in XRD and Raman spectra (as shown in Figs. 2 and 3). As the flow rate increases, a nearly-two order magnitude change in resistance is observed in the samples which are deposited in 5, 10, and 30 sccm as shown in Fig. 7(b). However, the steepness of the transitions is found to be gradual with very narrow hysteresis. The reason for observing MIT in these three samples is the formation of the VO_2 (M1) phase (as shown in Figs. 2 and 3). Nevertheless, the relatively smaller grain size in all the three samples (as shown in Fig. 4(c), (d) and (e)) reduces the transition temperature and makes the transition sluggish, which is also observed by Miller et al. [46] It has been argued that higher densities of grain boundaries (in other words smaller grain size) would enhance the availability of nucleating defects, which in turn would decrease the hysteresis as also observed here. Further increase in flow rate while depositing the film (i.e. the samples which are grown in 50 and 90 sccm) show a more than two orders of magnitude change in resistance with the function of temperature as depicted in Fig. 7(c). Also, the transition temperature has proceeded further as compared to the sample deposited in 5, 10 and 30 sccm. The reason is also similar in this case. As the grain size of the samples (which are deposited in 50 and 90 sccm flow rate) becomes larges (Fig. 4(f, g) 5(f, g)) with increasing flow rate, the transition temperature becomes higher and the hysteresis width increases. Careful observation delineates sample deposited in a 50 sccm flow rate are smaller in grain size and therefore, show a much higher change in resistance than the sample deposited in 90 sccm.

Table 2
Magnitude (Ω), hysteresis width (Δ°C), and position (°C) of the metal–insulator transition for vanadium dioxide (VO_2) deposited at different flow rate condition.

Sample	Magnitude	Hysteresis width (°C)	Position (°C)
0.5 sccm	$10^{0.1}$	Almost no hysteresis	No transition
1 sccm	$10^{0.3}$	Almost no hysteresis	No Transition
5 sccm	$10^{2.0}$	8	43.1
10 sccm	$10^{1.6}$	6	33.6
30 sccm	$10^{2.1}$	5.8	37.1
50 sccm	$10^{2.7}$	10.1	58.9
90 sccm	$10^{2.1}$	13.3	54.4

It should be also noted that in all the cases after the transition when VO_2 appears to be a metallic phase, the resistance of this phase decreases when further increasing the temperature, which is counter intuitive as per the behavior of an ideal metal. The reason is that the metallic state of VO_2 is degenerate semiconducting in nature. It has already been reported that electron scattering in the metallic phase of VO_2 by phonons is insignificant at 85 °C (well beyond the transition), which indicates that the resistance of the VO_2 at the metallic state does not increase with the function of temperature [47].

It is important to mention that all the samples deposited here have a tiny amount of crystalline V_2O_3 present as an impurity in the VO_2 matrix. The XPS results also support the presence of V_2O_3. Further, the XPS depicts the presence of V_2O_5 phases, however it is either on the surface or in an amorphous state as XRD is not able to resolve its crystalline feature. Nonetheless, there is a mixed phase possible in all the cases which might influence the transition behavaior. Although we believe their effect is not significant as compared to the effect of stress, the grain size, grain size distribution and grain boundaries.

Further, it is worth noting that in all the cases the transition temperature is much below than 68 °C which is well reported for single crystal VO_2 [13,48]. The reason is all the samples studied here are of poly crystalline in nature comprised of lots of grains and grain

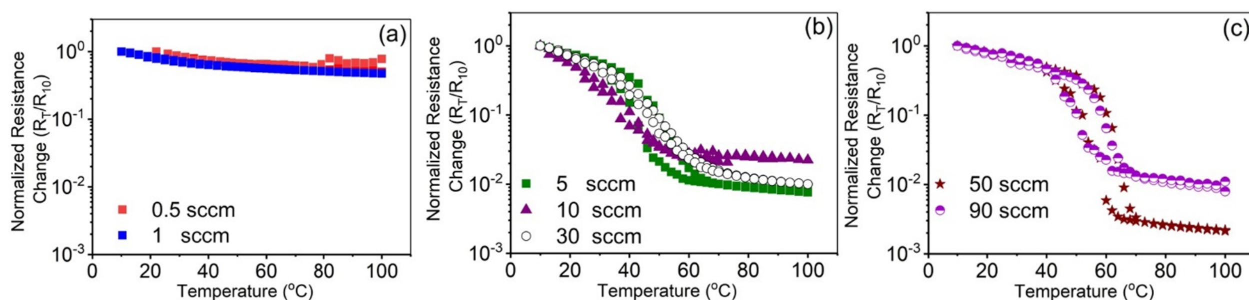

Fig. 7. Resistance as a function of temperature for vanadium dioxide thin films grown at different flow rates i.e. (a) at 0.5 and 1 sccm, (b) at 5, 10 and 30 sccm, and (c) 50 and 90 sccm.

Table 3
Experimental and theoretical *d* spacing (A°) for the observed lattice planes (011).

Sample	d $_{spacing}$ (theoretical)	d $_{spacing}$ (actual)*	Strain type
0.5 sccm	3.2067	3.1870	Compressive
1 sccm	3.2067	3.1831	Compressive
5 sccm	3.2067	3.1831	Compressive
10 sccm	3.2067	3.1963	Compressive
30 sccm	3.2067	3.1936	Compressive
50 sccm	3.2067	3.1870	Compressive
90 sccm	3.2067	3.1976	Compressive

*d $_{spacing}$ (actual) is calculated from (011) plane of Fig. 2.

boundaries which in turn reduces the transition as described earlier [46]. Moreover, it should be also noted all the samples (specifically 30, 50 and 90 sccm) discussed in this study which are found to be well crystalline VO_2 (M1) phase and are in compressive stress with respect to the ideal d-spacing of the signature peak i.e. (011) of polycrystalline VO_2 as shown in Table 3. Park et al. and Aetukuri et al. showed that the compressive stress in VO_2 reduces the transition temperature further towards the lower end by controlling the orbital occupancy [38,49].

It is well known that in PLD when high energy lasers interacts with the target material (in this case V-metal), it vaporizes the material and forms a plasma plume. In the presence of external gas (in this case O_2) the metal-rich plasma interacts with oxygen and can form nascent oxygen atom, ions, clusters, etc [44].

The reaction between highly active oxygen atom, ions, and vanadium metal can form vanadium oxide and deposit onto the substrate. It has been observed, as discussed earlier, that at $P_{O2} \sim 50$ mTorr, and at the other above conditions that the formation of high quality VO_2 occurs however, Q_{O2} plays a critical role. Although in this case the Knudsen number ~0.02 (the number 0.02 indicates intermediate flow regime) is the same for any flow rate used here, it affects the interaction of oxygen moieties and metal (vanadium) plasma plumes thereby controlling the diffusion of oxygen at the metal surface. This diffusion process depends on how fast the oxygen is being pumped through the chamber. As a result it allows more time for the oxygen plasma to diffuse in the metal substrate which can lead to the formation of an oxygen-rich phase of vanadium oxide. An optimum flow rate is expected to facilitate the diffusion process and can make the deposition process more economical because the user may not be pumping away too much oxygen during the film deposition.

4. Conclusion

In this work, we have deposited vanadium dioxide thin films onto a thermal oxide (Si/SiO_2) substrate using the PLD technique at different oxygen flow rates (0.5 to 90 sccm) keeping a constant background pressure ($P_{O2} \sim 50$ mTorr) of oxygen. Deposited films were further characterized by various techniques in order to understand the effect of the oxygen flow rate in the chamber during the deposition of the films. X-ray diffraction measurements revealed the existence of VO_2 (M1) polycrystalline phase in all samples, however the quality of crystallinity was improved with increasing flow rates. Raman measurement also showed a similar trend with increasing flow rates. SEM and AFM show, by and large, grain growth occurs in the samples with increasing flow rates, and so does the surface roughness. XPS show some sort of mixed trend in the valence state of vanadium that is observed with increasing flow rates. Samples deposited at lower (0.5 and 1 sccm) and higher flow rates (50 and 90 sccm) show an admixture of V^{4+} and V^{3+} states whereas samples deposited at intermediate flow rates (5, 10 and 30 sccm) show admixture ofV^{5+}, V^{4+}, and V^{3+} states. Finally, temperature-dependent resistance measurements show different characteristics with increasing flow rates. No transition was observed for samples deposited with low oxygen flow rates (0.5 and 1 sccm). However, a gradual transition was observed for the samples deposited in the intermediate flow rate regime (5, 10 and 30 sccm) where transition temperature lies within 33 to 43 °C. Additionally, the transition magnitude varies from 1.6 to 2 orders with 5 to 8 °C hysteresis width. Further, with increasing flow rate (50 and 90 sccm) the magnitude of the transition became even higher (almost 3 orders of magnitude for 50 sccm), although the sample deposited at 90 sccm suffers from the magnitude of change in resistance. The onset of transition in both the samples proceeded to higher temperature with thicker hysteresis. This happens due to the grain size of the samples becoming larger with increasing flow rate. From the above study it is clearly discernible that in order to tune the transition characteristics of vanadium dioxide thin film, the flow rate is also important criteria along with the background pressure. Very low flow rate will not show any transition (0.5 and 1 sccm), intermediate flow rate (5 to 30 sccm) will show gradual transition with shallow hysteresis with the low onset of transition temperature whereas a higher flow rate will show a sharper transition with a large magnitude change in resistance (nearly-three orders) with the higher onset of transition temperature and thicker hysteresis width. Here we argue that the diffusion of oxygen might play a critical role because of the flow rate, however true mechanism demands a thorough theoretical study.

CRediT authorship contribution statement

Syed A. Bukhari: Methodology, Validation, Formal analysis, Investigation, Writing - original draft. **Sooraj Kumar:** Formal analysis, Visualization. **Pawan Kumar:** Formal analysis, Visualization. **Sarang P. Gumfekar:** Methodology. **Hyun-Joong Chung:** Resources. **Thomas Thundat:** Resources, Funding acquisition. **: .** **Ankur Goswami:** Conceptualization, Visualization, Writing - original draft, Supervision, Project administration, Funding acquisition.

Declaration of Competing Interest

The authors declare that they have no known competing financial interests or personal relationships that could have appeared to influence the work reported in this paper.

Acknowledgements

This work was supported by the Canada Excellence Research Chair (CERC) Program (ID: SF0926 and grant number: RES 0006296). AG acknowledges IIT Delhi for providing the seed grant (PLN12/04 MS) to do some of the electrical measurements in his lab. The authors acknowledge the characterization facilities provided by the Nanofab at the University of Alberta. Ms. Rosmi Abraham is also gratefully acknowledged for helping to run the electrical measurements.

Appendix A. Supplementary data

Supplementary data to this article can be found online at https://doi.org/10.1016/j.apsusc.2020.146995.

References

[1] S. Catalano, M. Gibert, J. Fowlie, J. Íñiguez, J.M. Triscone, J. Kreisel, Rare-earth nickelatesRNiO$_3$: thin films and heterostructures, Rep. Prog. Phys 81 (2018) 046501.
[2] B. Torriss, J. Margot, M. Chaker, Metal-insulator transition of strained SmNiO$_3$ thin films: structural, electrical and optical properties, Sci. Rep. 7 (2017) 40915.
[3] F.J. Morin, Oxides which show a metal-to-insulator transition at the neel temperature, Phys. Rev. Lett. 3 (1959) 34–36.
[4] K. Liu, S. Lee, S. Yang, O. Delaire, J. Wu, Recent progresses on physics and applications of vanadium dioxide, Mater. Today 21 (2018) 875–896.
[5] S. Autier-Laurent, B. Mercey, D. Chippaux, P. Limelette, C. Simon, Strain-induced pressure effect in pulsed laser deposited thin films of the strongly correlated oxide V_2O_3, Phys. Rev. B 74 (2006) 195109.
[6] A. Rúa, R. Cabrera, H. Coy, E. Merced, N. Sepúlveda, F.E. Fernández, Phase transition behavior in microcantilevers coated with M1-phase VO_2 and M2-phase VO_2: Cr thin films, J. Appl. Phys. 111 (2012) 104502.
[7] M.A. Kats, R. Blanchard, S. Zhang, P. Genevet, C. Ko, S. Ramanathan, F. Capasso, Vanadium dioxide as a natural disordered metamaterial: perfect thermal emission and large broadband negative differential thermal emittance, Phys. Rev. X 3 (2013) 041004.
[8] S.-C. Chen, H.-K. Yuan, Z.-H. Zhai, L.-H. Du, S.-C. Zhong, H.-F. Zhu, Q.-W. Shi, W.-X. Huang, Z.-R. Li, L.-G. Zhu, All optically driven memory device for terahertz waves, Opt. Lett. 45 (2020) 236–239.
[9] R. Molaei, R. Bayati, S. Nori, D. Kumar, J.T. Prater, J. Narayan, Diamagnetic to ferromagnetic switching in VO_2 epitaxial thin films by nanosecond excimer laser treatment, Appl. Phys. Lett. 103 (2013) 252109.
[10] R. McGee, A. Goswami, R. Abraham, S. Bukhari, T. Thundat, Phase transformation induced modulation of the resonance frequency of VO_2/TiO_2 coated microcantilevers, MRS Adv. 3 (2018) 359–364.
[11] M.M. Qazilbash, M. Brehm, B.-G. Chae, P.-C. Ho, G.O. Andreev, B.-J. Kim, S.J. Yun, A.V. Balatsky, M.B. Maple, F. Keilmann, H.-T. Kim, D.N. Basov, Mott transition in VO_2 revealed by infrared spectroscopy and nano-imaging, Science 318 (2007) 1750–1753.
[12] H.-T. Kim, B.-G. Chae, D.-H. Youn, S.-L. Maeng, G. Kim, K.-Y. Kang, a.Y.-S. Lim, Mechanism and observation of Mott transition in VO2-based two- and three-terminal devices, New J. Phys. 6 (2004): 1–20.
[13] S. Lee, I.N. Ivanov, J.K. Keum, H.N. Lee, Epitaxial stabilization and phase instability of VO_2 polymorphs, Sci. Rep. 6 (2016) 19621.
[14] R. Shi, N. Shen, J. Wang, W. Wang, A. Amini, N. Wang, C. Cheng, Recent advances in fabrication strategies, phase transition modulation, and advanced applications of vanadium dioxide, Appl. Phys. Rev. 6 (2019) 011312.
[15] J. Zhou, Y. Gao, Z. Zhang, H. Luo, C. Cao, Z. Chen, L. Dai, X. Liu, VO_2 thermochromic smart window for energy savings and generation, Sci. Rep. 3 (2013) 3029.
[16] R. McGee, A. Goswami, S.A.M. Bukhari, L. Zhou, K. Shankar, T. Thundat, Fabrication of phase change microstring resonators via top down lithographic techniques: incorporation of VO_2/TiO_2 into conventional processes, J. Microelectromech. Syst. 28 (2019) 766–775.
[17] S.A. Bukhari, A. Goswami, R. McGee, R. Abraham, D. Hume, H.J. Chung, T. Thundat, Bidirectional frequency tuning of vanadium dioxide (VO2) microstring resonator by optothermal excitation, in: 2020 IEEE 33rd International Conference on Micro Electro Mechanical Systems (MEMS), 2020, pp. 961–964.
[18] A. Younis, D. Chu, S. Li, Oxygen level: the dominant of resistive switching characteristics in cerium oxide thin films, J. Phys. D: Appl. Phys 45 (2012) 355101.
[19] B. Zhi, G. Gao, H. Xu, F. Chen, X. Tan, P. Chen, L. Wang, W. Wu, Electric-field-modulated nonvolatile resistance switching in VO_2/PMN-PT(111) heterostructures, ACS Appl. Mater. Interfaces 6 (2014) 4603–4608.
[20] B. Wang, J. Lai, H. Li, H. Hu, S. Chen, Nanostructured vanadium oxide thin film with high TCR at room temperature for microbolometer, Infrared Phys. Technol. 57 (2013) 8–13.
[21] E. Strelcov, Y. Lilach, A. Kolmakov, Gas sensor based on metal−insulator transition in VO_2 nanowire thermistor, Nano Lett. 9 (2009) 2322–2326.
[22] O. Ojelere, D. Graf, T. Ludwig, N. Vogt, A. Klein, S. Mathur, Reductive transformation of V(iii) precursors into vanadium(ii) oxide nanowires, Dalton Trans. 47 (2018) 6842–6849.
[23] Y. Zhang, J. Zhang, X. Zhang, Y. Deng, Y. Zhong, C. Huang, X. Liu, X. Liu, S. Mo, Influence of different additives on the synthesis of VO_2 polymorphs, Ceram. Int. 39 (2013) 8363–8376.
[24] A. Srivastava, H. Rotella, S. Saha, B. Pal, G. Kalon, S. Mathew, M. Motapothula, M. Dykas, P. Yang, E. Okunishi, D.D. Sarma, T. Venkatesan, Selective growth of single phase VO_2(A, B, and M) polymorph thin films, APL Mater. 3 (2015) 026101.
[25] D. Bhardwaj, A. Goswami, A.M. Umarji, Synthesis of phase pure vanadium dioxide (VO_2) thin film by reactive pulsed laser deposition, J. Appl. Phys. 124 (2018) 135301.
[26] B. Rajeswaran, A.M. Umarji, Defect engineering of VO_2 thin films synthesized by chemical vapor deposition, Mater. Chem. Phys. 245 (2020) 122230.
[27] J. Yoon, C. Park, S. Park, B.S. Mun, H. Ju, Correlation between surface morphology and electrical properties of VO_2 films grown by direct thermal oxidation method, Appl. Surf. Sci. 353 (2015) 1082–1086.
[28] H. Liu, D. Wan, A. Ishaq, L. Chen, B. Guo, S. Shi, H. Luo, Y. Gao, Sputtering deposition of sandwich-structured V_2O_5/Metal (V, W)/V_2O_5 Multilayers For The Preparation Of High-Performance Thermally Sensitive VO_2 thin films with selectivity of VO_2 (B) and VO_2 (M) polymorph, ACS Appl. Mater. Interfaces 8 (2016) 7884–7890.
[29] H. Zhang, Z. Wu, D. Yan, X. Xu, Y. Jiang, Tunable hysteresis in metal-insulator transition of nanostructured vanadium oxide thin films deposited by reactive direct current magnetron sputtering, Thin Solid Films 552 (2014) 218–224.
[30] A. Kaushal, N. Choudhary, N. Kaur, D. Kaur, VO_2–WO_3 nanocomposite thin films synthesized by pulsed laser deposition technique, Appl. Surf. Sci. 257 (2011) 8937–8944.
[31] N. Émond, A. Hendaoui, A. Ibrahim, I. Al-Naib, T. Ozaki, M. Chaker, Transmission of reactive pulsed laser deposited VO_2 films in the THz domain, Appl. Surf. Sci. 379 (2016) 377–383.
[32] D. Dijkkamp, T. Venkatesan, X.D. Wu, S.A. Shaheen, N. Jisrawi, Y.H. Min-Lee, W.L. McLean, M. Croft, Preparation of Y-Ba-Cu oxide superconductor thin films using pulsed laser evaporation from high Tc bulk material, Appl. Phys. Lett. 51 (1987) 619–621.
[33] M. Borek, F. Qian, V. Nagabushnam, R.K. Singh, Pulsed laser deposition of oriented VO_2 thin films on R-cut sapphire substrates, Appl. Phys. Lett 63 (1993) 3288–3290.
[34] D.H. Kim, H.S. Kwok, Pulsed laser deposition of VO_2 thin films, Appl. Phys. Lett 65 (1994) 3188–3190.
[35] Y.X. Guo, Y.F. Liu, C.W. Zou, Z.M. Qi, Y.Y. Wang, Y.Q. Xu, X.L. Wang, F. Zhang, R. Zhou, Oxygen pressure induced structure, morphology and phase-transition for VO_2/c-sapphire films by PLD, Appl. Phys. A 115 (2014) 1245–1250.
[36] L.L. Fan, Y.F. Wu, C. Si, C.W. Zou, Z.M. Qi, L.B. Li, G.Q. Pan, Z.Y. Wu, Oxygen pressure dependent VO_2 crystal film preparation and the interfacial epitaxial growth study, Thin Solid Films 520 (2012) 6124–6129.
[37] E.-K. Koussi, F. Bourquard, T. Tite, D. Jamon, F. Garrelie, Y. Jourlin, Synthesis of vanadium oxides by pulsed laser deposition and rapid thermal annealing, Appl. Surf. Sci. 146267 (2020).
[38] R. McGee, A. Goswami, S. Pal, K. Schofield, S.A.M. Bukhari, T. Thundat, Sharpness and intensity modulation of the metal-insulator transition in ultrathin VO_2 films by interfacial structure manipulation, Phys. Rev. Mat. 2 (2018) 034605.
[39] R. McGee, A. Goswami, B. Khorshidi, K. McGuire, K. Schofield, T. Thundat, Effect of process parameters on phase stability and metal-insulator transition of vanadium dioxide (VO_2) thin films by pulsed laser deposition, Acta Mater. 137 (2017) 12–21.
[40] D. Bhardwaj, D.K. Singh, S.B. Krupanidhi, A.M. Umarji, Fabrication of smooth thin film of vanadium oxides (VO_x) using pulsed laser deposition, Appl. Phys. A 126 (2020) 157.
[41] S. Yu, S. Wang, M. Lu, L. Zuo, A metal-insulator transition study of VO_2 thin films grown on sapphire substrates, J. Appl. Phys. 122 (2017) 235102.
[42] R.T. Kivaisi, M. Samiji, Optical and electrical properties of vanadium dioxide films prepared under optimized RF sputtering conditions, Sol. Energy Mater. Sol. 57 (1999) 141–152.
[43] S. Kittiwatanakul, J.D.N. Laverock Jr, K.E. Smith, S.A. Wolf, J. Lu, Transport behavior and electronic structure of phase pure VO_2 thin films grown on c-plane sapphire under different O_2 partial pressure, J. Appl. Phys. 114 (2013) 053703.
[44] J. Konno, A. Nezu, H. Matsuura, H. Akatsuka, Excitation kinetics of oxygen O(1D) state in low-pressure oxygen plasma and the effect of electron energy distribution function, J. Adv. Oxidation. Technol. (2017).
[45] T. Kimoto, H. Matsunami, Surface diffusion lengths of adatoms on 6H-SiC{0001} faces in chemical vapor deposition of SiC, J. Appl. Phys. 78 (1995) 3132–3137.
[46] M.J. Miller, J. Wang, Influence of grain size on transition temperature of thermochromic VO_2, J. Appl. Phys. 117 (2015) 034307.
[47] D. Fu, K. Liu, T. Tao, K. Lo, C. Cheng, B. Liu, R. Zhang, H.A. Bechtel, J. Wu,

Comprehensive study of the metal-insulator transition in pulsed laser deposited epitaxial VO_2 thin films, J. Appl. Phys. 113 (2013) 043707.

[48] B.S. Mun, K. Chen, Y. Leem, C. Dejoie, N. Tamura, M. Kunz, Z. Liu, M.E. Grass, C. Park, J. Yoon, Y.Y. Lee, H. Ju, Observation of insulating–insulating monoclinic structural transition in macro-sized VO_2 single crystals, Phys. Status Solidi RRL 5 (2011) 107–109.

[49] J.H. Park, J.M. Coy, T.S. Kasirga, C. Huang, Z. Fei, S. Hunter, D.H. Cobden, Measurement of a solid-state triple point at the metal–insulator transition in VO_2, Nature 500 (2013) 431.

[50] Hao Wu, Qiang Fu, Xinhe Bao, In situ Raman spectroscopy study of metal-enhanced hydrogenation and dehydrogenation of VO_2, J. Phys.: Condens. Matter. 28 (2016) 434003, https://doi.org/10.1088/0953-8984/28/43/434003.